ORIGINAL RESEARCH

Development of ^{99m}Tc-radiolabeled nanosilica for targeted detection of HER2-positive breast cancer

Paolo Rainone[1,2,*]
Benedetta Riva[3,*]
Sara Belloli[1]
Francesco Sudati[4]
Marilena Ripamonti[1]
Paolo Verderio[3]
Miriam Colombo[3]
Barbara Colzani[3]
Maria Carla Gilardi[1]
Rosa Maria Moresco[5]
Davide Prosperi[3]

[1]Institute of Molecular Bioimaging and Physiology, CNR, Segrate (MI), [2]Doctorate School of Molecular and Translational Medicine, University of Milan, Milan, [3]NanoBioLab, Dipartimento di Biotecnologie e Bioscienze, Università di Milano-Bicocca, Milano, [4]PET and Nuclear Medicine Unit, San Raffaele Scientific Institute, Milan, [5]Department of Medicine and Surgery, University of Milano-Bicocca, Monza, Italy

*These authors contributed equally to this work

Correspondence: Sara Belloli
Institute of Molecular Bioimaging and Physiology of CNR, Via Fratelli Cervi 93, 20090 Segrate, Italy
Tel +39 02 2643 3640
Fax +39 02 2643 2717
Email belloli.sara@hsr.it

Davide Prosperi
NanoBioLab, Dipartimento di Biotecnologie e Bioscienze, Università di Milano-Bicocca, Piazza della Scienza 2, 20126 Milano, Italy
Tel +39 02 6448 3302
Fax +39 02 6448 3565
Email davide.prosperi@unimib.it

Abstract: The human epidermal growth factor receptor 2 (HER2) is normally associated with a highly aggressive and infiltrating phenotype in breast cancer lesions with propensity to spread into metastases. In clinic, the detection of HER2 in primary tumors and in their metastases is currently based on invasive methods. Recently, nuclear molecular imaging techniques, including positron emission tomography and single photon emission computed tomography (SPECT), allowed the detection of HER2 lesions in vivo. We have developed a ^{99m}Tc-radiolabeled nanosilica system, functionalized with a trastuzumab half-chain, able to act as drug carrier and SPECT radiotracer for the identification of HER2-positive breast cancer cells. To this aim, nanoparticles functionalized or not with trastuzumab half-chain, were radiolabeled using the ^{99m}Tc-tricarbonyl approach and evaluated in HER2 positive and negative breast cancer models. Cell uptake experiments, combined with flow cytometry and fluorescence imaging, suggested that active targeting provides higher efficiency and selectivity in tumor detection compared to passive diffusion, indicating that our radiolabeling strategy did not affect the nanoconjugate binding efficiency. Ex vivo biodistribution of ^{99m}Tc-nanosilica in a SK-BR-3 (HER2^{+}) tumor xenograft at 4 h postinjection was higher in targeted compared to nontargeted nanosilica, confirming the in vitro data. In addition, viability and toxicity tests provided evidence on nanoparticle safety in cell cultures. Our results encourage further assessment of silica ^{99m}Tc-nanoconjugates to validate a safe and versatile nanoreporter system for both diagnosis and treatment of aggressive breast cancer.

Keywords: SPECT, targeted radionuclide imaging, silica nanoparticles, TZ-half chain conjugation, ^{99m}Tc-tricarbonyl radiolabeling

Introduction

Breast cancer (BC) is the most common tumor in women, being the second cause of death because of cancer.[1] BCs overexpressing the human epidermal growth factor receptor 2 (HER2) account for 30% of invasive breast tumors and are associated with an aggressive biological behavior translating to poorer clinical outcomes.[2] The development of trastuzumab (TZ), a recombinant humanized monoclonal antibody that recognizes the extracellular domain of the HER2 protein, has dramatically altered the natural history of HER2-positive (HER2^{+}) BC and ranks among the most significant advances in cancer therapeutics.[3,4] Nevertheless, in order to have a benefit from TZ or related therapies, the detection of HER2 expression remains a fundamental issue. Nowadays, HER2 expression is evaluated in postsurgery or bioptic specimen by immunohistochemistry (IHC) or fluorescence in situ hybridization[5] on the primary lesion. Molecular imaging techniques such as positron emission tomography (PET) and single photon emission computed tomography (SPECT) allow the in vivo detection of molecular targets during tumor progression and diffusion.[6] These radionuclide-based

imaging techniques can be exploited to visualize and quantify the presence/absence of biological markers by means of specific radiolabeled probes, administered at tracer dose.[7] Hence, these techniques may allow the assessment of HER2 expression both in primary and secondary lesions not amenable to biopsy.[8] Among the radionuclides currently used in nuclear medicine for radiolabeling, ^{99m}Tc offers the advantage of safety and easy availability thanks to the presence of clinical grade generators. In addition, due to its chemical properties, it can be coordinated in a stable oxidation state by bi- and tridentate ligands represented either by small functional linkers, such as hydrazinonicotinic acid[9] and nitrilotriacetic acid,[10] or by aminoacidic residues, such as histidine and cysteine.[11] Recent advances in nanobiotechnology have led to the development of nanoparticles (NPs) that are able to host various functionalities and to be loaded with the therapeutic molecules, hence making it possible to have simultaneous diagnosis and treatment of human cancers (theranostics).[12] Significant advantages are offered by the use of NP systems compared to direct treatment administration. First, the delivery of cytotoxic agents to cancer cells allows to decouple the side effects of systemic chemotherapy from the therapeutic effects, getting high drug bioavailability at the tumor site,[13] improved therapeutic efficiency and minimal influence on normal cells.[14] Moreover, it is possible to label the NPs with radioactive and/or fluorescent probes for imaging detection, without affecting the therapeutic activity, while gaining high signal-to-background ratio.[15] NPs can easily permeate the tumor vasculature and remain in tumors owing to the enhanced permeability and retention (EPR) effect,[16] but this passive diffusion is not enough to improve the selectivity in the NPs interaction with cancer cells.[17] Recently, various ligands that can specifically bind to receptors overexpressed in cancer cells, including peptides and antibodies, have been coengineered with smart nanomaterials for the design and construction of novel drug delivery systems and targeted diagnostic probes.[18,19] Silica NPs (SiNPs) possess high biocompatibility and their functionalization with monoclonal antibodies (eg, TZ for HER2+ BC) can be a useful tool for both tumor imaging and targeted chemotherapy.[20] In addition, these NPs are intrinsically hydrophilic, easy and inexpensive to prepare and can be chemically modified in a straightforward manner. SiNPs are optically transparent in the near-infrared (NIR), visible and ultraviolet regions,[21] which is particularly favorable for in vivo imaging. For all these reasons, SiNPs have been recently employed as detection probes in imaging studies, including PET/SPECT, MRI and/or fluorescence (mostly

NIRF) imaging, and as nanocarriers for the treatment of several types of cancer in animal models. SiNPs have been differently synthetized and functionalized to target specific tumor phenotypes (eg, colon, breast, gut) or associated features (eg, neoangiogenesis).[22–24] In this study, we explored the use of multifunctional [99m]Tc SiNPs for early detection of HER2+ BC lesions using a novel radiolabeling approach. Spherical SiNPs (hydrodynamic size =100 nm) were engineered with anti-HER2 monoclonal antibody in the form of a TZ half-chain (Hc-TZ) and radiolabeled employing ^{99m}Tc for SPECT imaging. SiNPs were also labeled in with the fluoresceine isothiocyanate (FITC) dye to allow for NP detection by fluorescence microscopy. The aim of this work was to investigate the contribution offered by active targeting to the distribution of NPs in solid BC lesions and in cell internalization, in comparison to nonspecifically targeted SiNPs. Moreover, we set up and tested a radiolabeling procedure that allowed us to follow in vivo tumor uptake and organ kinetics distribution of nanosilica, using nuclear medicine techniques. This SiNPs system could be potentially used to develop a theranostic nanosystem combining noninvasive detection with an effective treatment for HER2+ breast cancer.

Materials and methods
Chemicals
All reagents and solvents were purchased from Sigma-Aldrich (St Louis, MO, USA), Rapp Polymere (Tuebingen, Germany), Riedel-de Haën (Seelze, Germany) and Fluka (St Gallen, Germany) and used as received without further purification. TZ antibody was purchased by Genentech (Herceptin®; Genentech, South San Francisco, CA, USA) and used after dialysis in phosphate-buffered saline (PBS) at 4°C on a Slyde-A-Lyzer dialysis cassette (Waltham, MA, USA) with a 7 kDa cutoff. Ultrasounds were generated by S15H Elmasonic Apparatus (Elma, Singen, Germany).

Synthesis of IPTES-NTA complex
IPTES (2 μL) was mixed with a solution of NTA (2 mg) in 200 μL of deionized water:ethanol (9:1). The reaction was left under stirring for 2 h at room temperature (RT) and the complex was used immediately after preparation.

Preparation of TZ half-chain
Cysteamine (28 mM) was dissolved in a reaction buffer (20 mM Hepes, 5 mM ethylenediaminetetraacetic acid [EDTA], pH 7.2, 1 mL) and dialyzed TZ (1 mg) in PBS, pH 7.2, was added. The solution was incubated under gentle stirring at 37°C for 90 min. The reaction was cooled to RT

and purified using a Sephadex PD10 column. TZ half-chain was used immediately after purification.

Synthesis of fluorescent core-shell SiNPs

Monodisperse fluorescent silica nanospheres were obtained by Stöber synthesis. In brief, to a NH_4OH solution in water (1.827 g, 0.58 M), dry ethanol was added to reach a total volume of 50 mL and the mixture was mixed under magnetic stirring. To the above solution, tetraethyl orthosilicate (TEOS) (1.990 mL, 0.17 M) and APTMS-FITC complex (1 mL)[25] were rapidly added and the reaction was stirred for 20 h at RT in the darkness. The solvent was then evaporated under reduced pressure and deionized water was added to give a final particle concentration of 10 mg/mL (concentration determined by drying 1 mL of NPs suspension at 100°C). To the SiNPs suspension, L-arginine (0.5 mg/mL) was added and the solution was equilibrated to 70°C for 10 min. Next, TEOS (765 µL) was slowly added and the reaction was left under mild stirring at 70°C overnight in the darkness. The resulting core-shell NPs were washed three times (20,000 rcf, 20 min) and redispersed with deionized water to a final concentration of 10 mg/mL.

Synthesis of SiNP-NTA-TZ

Step 1 – Amination and IPTES-NTA conjugation to core-shell NPs

To a desired amount of core-shell NPs, glacial acetic acid (5.25 µmol/mg of NPs), IPTES-NTA (4 nmol/mg of NPs) and APTMS (1.72 µmol/mg of NPs) were added in sequence. The reaction was left under vigorous stirring for 2 h, after which the aminated NPs were washed three times with ultrapure water and twice with 20 mM Hepes buffer, pH 9, and redispersed in the same buffer (10 mg/mL) for further functionalization.

Step 2 – Introduction of polyethylene glycol (PEG)-OMe

To the NPs suspension in Hepes, $MS(PEG)_4$ was added in an equimolar amount with respect to the surface amine functionalities assessed by ninhydrin assay. The reaction was left under stirring for 2 h, after which the NPs were washed (20,000 rcf, 20 min) twice with ultrapure water and twice with 20 mM Hepes buffer, pH 7.4 and redispersed in the same buffer for the next steps.

Step 3 – Introduction of PEG-Mal

$SM(PEG)_8$ was added to the NPs suspension in a fivefold molar excess with respect to the unreacted surface amine functionalities assessed by ninhydrin assay. The reaction was left under stirring for 2 h, after which the NPs were washed

once with ultrapure water and then redispersed in 20 mM Hepes buffer, pH 7.4.

Step 4 – TZ half-chain coupling

To the NPs suspension, the previously prepared TZ half-chain was added (10 µg/mg of NPs) and the reaction was left under gentle stirring for 2 h. After the reaction, the NPs were washed (16,000 rcf, 20 min, 4°C) once with 20 mM Hepes, pH 7.4 and resuspended in the same buffer.

Step 5 – Saturation of free maleymido-groups

To the NPs suspension, $MT(PEG)_4$, (0.5 µg/mg of NPs) was added and the reaction was left under stirring for 1 h, after which the NPs were washed (16,000 rcf, 20 min, 4°C) three times with 20 mM Hepes, pH 7.4 and resuspended in 1 mM $NiCl_2$, pH 8.

Step 6 – Nickel chelation to NTA

The NPs were incubated under stirring in the $NiCl_2$ buffer for 1 h, and then washed (16,000 rcf, 20 min, 4°C) twice with 20 mM Hepes pH 7.5 and resuspended in the same buffer. Each sample of NPs was analyzed by UV-visible spectroscopy and absorbance values were taken at the maximum absorbance peak of FITC (λ =485 nm). Those values were used to derive the sample concentration by means of a calibration curve previously set up by known concentrations of core-shell NPs.

Synthesis of SiNP, SiNP-TZ and SiNP-NTA

The other NPs used in this study were synthesized as described in the previous section, avoiding some steps: in particular, the conjugation of IPTES-NTA, steps 4 and 6 for SiNP, the conjugation of IPTES-NTA and step 6 for SiNP-TZ, step 4 for SiNP-NTA.

Determination of amino groups: ninhydrin assay

Our protocol was adapted from a standard method described in the literature.[26] In brief, aminated SiNPs (1 or 2 mg in 400 µL of dry ethanol) were incubated with 100 µL of ninhydrin stock solution (4 mg/mL in dry ethanol). The reaction was heated at 60°C for 1 h. After cooling to RT, NPs were separated from the supernatant by centrifugation (20,000 rcf) and an aliquot of the particle-free blue supernatant read with UV-Vis spectrophotometer at 570 nm. A standard calibration curve was created using ethanolamine in a concentration range between 0 and 3 mM in dry ethanol.

NPs characterization

Dynamic light scattering measurements were performed with Zetasizer Nano ZS ZEN3600 (Malvern Instruments Ltd, Worcestershire, UK), equipped with a He–Ne laser (λ =632.8 nm) working at 4 mW. A disposable cuvette with an optical length of 1 cm was used and scattered light was collected at 173°. The samples were prepared with an average concentration of 100 μg/mL in ultrapure water, and they were allowed to equilibrate at 25°C for 30 s before the analysis. The hydrodynamic diameter was derived using Stokes–Einstein equation, considering a viscosity of the medium of 0.8872 cP. The results are reported as z-average. ζ-Potential measurements were performed with the same instruments, analyzing the electrophoretic light scattering of samples. ζ-Potential values were calculated by the Zetasizer Software based on electrophoretic mobility and considering a viscosity of 0.8872 cP and a dielectric constant of 78.5. Samples were prepared with an average concentration of 100 μg/mL in 1 mM NaCl and they were allowed to equilibrate at 25°C for 30 s before the analysis. UV-Vis spectra were recorded by Nanodrop 2000C spectrophotometer (Thermo Fisher Scientific, Wilmington, Germany) in a range of wavelengths from 190 to 600 nm. The size and morphology of SiNP, SiNP-TZ, SiNP-NTA and SiNP-NTA-TZ were obtained using transmission electron microscopy (HT7700; Hitachi, Brugherio, Italy). In brief, a 25 μM of each sample was prepared in water and then 5.0 μL of each sample was dropped onto the copper grids and air-dried at 42°C.

Dot blot analysis

TZ presence on SiNP-TZ was evaluated through dot blot analysis. A total of 100 μL of SiNP-TZ was fixed on nylon membrane with Bio-Dot Microfiltration Apparatus (Bio-Rad, Hercules, CA, USA). As a reference, SiNP and core-shell NPs were used as control. Different amounts of TZ (150, 75, 37 ng) were spotted on the membrane and used as reference. After sample seeding, the membrane was blocked with PBS + bovine serum albumin (BSA) 2% for 1 h at RT under mild shaking, then incubated for 1 h with horse radish peroxidase-conjugated rabbit anti-human IgG polyclonal antibody (GeneTex inc., Irvine, CA, USA), diluted 1:20,000 in PBS + BSA 2%. The membrane was then washed three times with PBS +0.5% Tween 20 and the spots of TZ samples were visualized by enhanced chemiluminescence reagents (Westar Nova 2011; Cyanagen, Bologna, Italy). The light intensity of a single spot on the membrane was detected using Image Studio imaging system (Li-Cor, Lincoln, NE, USA).

Cell culture and animal models

All reagents and solvents were purchased from Sigma-Aldrich (St Louis, MO, USA) and Invitrogen Corp (Carls bad, CA, USA). The uptake of silica NPs (SiNP and SiNP-TZ) was studied using SK-BR-3 (HER2$^+$) and MDA-MB-468 (HER2$^-$) cell lines, obtained from ICLC Animal Cell Lines Database – Istituto Nazionale per la Ricerca sul Cancro IRCCS San Martino, Genova, Italy. Toxicity assay was also performed using MCF-10A (nontransformed mammary epithelial cell line) purchased from American Type Culture Collection (ATCC, Manassas, VA, USA). MDA-MB-468 and SK-BR-3 cells were maintained in Dulbecco's Modified Eagle's Medium (DMEM) (Sigma-Aldrich, Milan, Italy), high glucose, supplemented with 5% Penicillin/Streptomycin, 10% heat-inactivated fetal bovine serum (Euroclone S.p.A., Italy) and 2 mM L-glutamine. MCF-10A cells were cultured in Advanced DMEM medium (Thermo Fisher Scientific, Waltham, MA, USA) containing 10% heat-inactivated fetal bovine serum, 2 mM L-glutamine, 100 U/mL penicillin and 100 mg/mL streptomycin, 10 μg/mL Insulin (Sigma), 20 ng/mL epidermal growth factor (EGF; Sigma) and 0.5 μg/mL Hydrocortisol (Sigma).

Female Balb/c nude mice were obtained from the Envigo RMS S.r.l., Italy. Animal experiments were carried out in compliance with the institutional guidelines for the care and use of experimental animals, which have been notified to the Italian Ministry of Health and approved by the Ethics Committee of the San Raffaele Scientific Institute. Balb/c nude mice with the age of 7–8 weeks and weight of 24–26 g were maintained under specific pathogen free condition. To obtain SK-BR-3 tumor models, about 5×10^6 cells in 200 μL mixed solution (serum-free RMPI-1640 medium and matrigel at the volume ratio of 1:1) were injected under the right shoulder. Calipers were used to measure tumor volume (mm^3) two times per week and mice weight was recorded. Mice were randomized when tumor volumes reached an average of 100 mm^3.

In vitro binding efficiency and selectivity of SiNPs by flow cytometry

SK-BR-3 cells (HER2$^+$, 3×10^5) were incubated with 0.5 μg/mL of either SiNP, SiNP-TZ, SiNP-NTA or SiNP-NTA-TZ dispersed in serum free-DMEM. After different incubation times (20 min, 1 h, 4 h and 24 h), cells were washed twice with PBS and harvested in fluorescence-activated cell sorting (FACS) tubes. A total of 10^5 events were acquired for each analysis on FACS Calibur flow cytometer (Becton Dickinson, Milan, Italy) monitoring FITC emission (green fluorescence). Both the percentage of the fluorescent cells relative to the control (untreated cells) and the mean

fluorescent intensity of the fluorescence-positive cells were taken into account. The same experiment was performed with MDA-MB-468 cell line (HER2$^-$) as a negative control. The results were analyzed using FlowJo software.

In vitro fluorescence imaging of nonradiolabeled SiNPs

SK-BR-3 (HER2$^+$, 5×10^4) and MDA-MB-468 (HER2$^-$, 5×10^4) cells were grown on glass coverslips incubated with 0.025 mg of either SiNP, SiNP-TZ, SiNP-NTA or SiNP-NTA-TZ dispersed in cell culture media. After 20 min, 1 h, 4 h and 24 h of incubation at 37°C (humidified atmosphere, 5% CO$_2$ air), the medium was removed and cells were washed three times with PBS. The samples were fixed with methanol (at −20°C for 30 min) before fluorescence analysis; cell nuclei were counterstained by Hoechst (Thermo Fisher Scientific, Waltham, MA, USA) 1 µg/mL. The specific uptake of SiNPs in both cell lines was visualized by fluorescence microscopy (Nikon Eclipse 80i).

In vitro toxicity assay

In vitro cytotoxicity of the SiNPs was tested on SK-BR-3 (HER2$^+$), MDA-MB-468 (HER$^-$) and MCF10A (nontransformed mammary epithelial) lines through MTT assay,[27] and by viable cell counting on HER2 positive and negative cell lines.

During MTT test, both cell lines were seeded in 96-well plates (Corning, NY, USA) at a density of 5×10^3 cells per well and incubated for 48 h. The suspensions of SiNP, SiNP-TZ, SiNP-NTA or SiNP-NTA-TZ were diluted in culture medium at 50 µg/mL. The cell culture medium was then removed and replaced by 100 µL of fresh medium containing NPs. The cells were incubated for 1, 4, 24 and 48 h at 37°C in a humidified atmosphere, 5% CO$_2$ air. After the above times, medium was removed and 100 µL of MTT (5 mg/mL in PBS) was added to each well. After 3 h, the culture medium containing MTT solution was removed. A total of 100 µL of sodium dodecyl sulfate in 0.01M HCl solution was added to each well to dissolve the formazan crystals and then plates were analyzed using a microplate reader (SPECTROstar Omega – BMG LABTECH GmbH, Germany) at 570 nm.

During the viable cell counting experiments, NPs were incubated as described for the MTT test. The medium was removed from the samples and the cells were suspended in PBS 0.1M (5×10^5 cells/mL). A total of 10 µL of 0.4% Trypan blue was incubated for 3 min with the cell suspension (1:1), and then the mix was loaded on the Thoma chamber BLAUBRAND$^{(R)}$ (Sigma-Aldrich, Milan, Italy) for the counting of the unstained (viable) and stained (nonviable)

cells. Cell viability was expressed in both experiments by comparing the treated samples to cells incubated with normal culture medium which were considered to have 100% survival rate (% viability = [treated cells/control cells] ×100).[27] A threshold value of 60% was used to evaluate the sensitivity/resistance of cell lines to each NPs set, as recommended by the manufacturer.

Protocol for radiolabeling of SiNPs
Preparation of (^{99m}Tc[CO]$_3$)$^+$

The Isolink kit (Paul Scherrer Institut, Villigen, Switzerland) to prepare the labeling precursor ([^{99m}Tc(H$_2$O)$_3$(CO)$_3$]$^+$) contained the following lyophilized ingredients: 8.5 mg sodium tartrate, 2.85 mg sodium tetraborate decahydrate, 7.15 mg of sodium carbonate and 4.5 mg sodium bicarbonate. Freshly eluted ^{99m}TcO$_4^-$ from a commercial General Electric Healthcare, UK generator (~2 GBq) in 1 mL saline buffer was added to the kit vial and incubated at 100°C for 20 min. The vial was then allowed to cool to RT and the solution neutralized by adding stepwise 1M HCl to pH ~7 and then checked on pH paper (Merck Millipore, Milan, Italy). The radiochemical purity (RCP) of the product was analyzed by high performance liquid chromatography (HPLC) and RPC was greater than 95%.

(^{99m}Tc[CO]$_3$)$^+$-His-Tag prelabeling

An hexa-His-Tag peptide was prelabeled with (^{99m}Tc[CO]$_3$)$^+$. Conjugation of the hexa-His-Tag was almost quantitative and was performed by mixing 38 µL of peptide solution (5 mg/mL in Hepes buffer pH 7.4) to the (^{99m}Tc[CO]$_3$[OH$_2$]$_3$)$^+$ precursor solution. The solution mixture was incubated at RT under stirring for 60 min and then the % RCP was checked by HPLC and it was found to be greater than 95%.

Conjugation of (^{99m}Tc[CO]$_3$)$^+$-His-Tag to SiNP-NTA

The (^{99m}Tc[CO]$_3$)$^+$-His-Tag solution was added to 500 µL of SiNP-NTA NPs (6.7 mg/mL, 4 nmol NTA/mg SiNPs). The solution mixture was incubated at RT under stirring for 2.5 h and then the % RCP was checked. The solution was shaken for about 1 min on a vortex mixer and then centrifuged for 15 min at 18,000 rpm. Supernatant solution was withdrawn and the corresponding radioactivity was counted. The pellet was washed with Hepes buffer and centrifuged three times. After the measurement of radioactivity of total supernatant and pellet the % RCP was 42%.

Conjugation of (^{99m}Tc[CO]$_3$)$^+$-His-Tag to SiNP-NTA-TZ

The (^{99m}Tc[CO]$_3$)$^+$ His-Tag solution was added to 500 µL of SiNP-NTA-TZ NPs (8.6 mg/mL, 4 nmol NTA/mg SiNPs).

The solution mixture was incubated at RT under stirring for 2.5 h and then the % RCP was checked as described above and it was 23.8%.

Quality control

The chemical purity and RCP of each step of the synthesis was performed using an HPLC Akta system equipped with radiochemical flow counter (Bioscan, Eckert & Ziegler, Germany). For HPLC analysis of the radiolabeled ^{99m}Tc-tricarbonyl core and ^{99m}Tc-tricarbonyl-hexa-His peptide a Thermo Scientific BDS reverse-phase column (250×4.6) was used with a flow of 1.2 mL/min and a linear triphasic gradient of 2% B (MeOH) with A (0.1% TFA) from 0 to 10′min, 2% C (CH$_3$CN 50%+0.1% TFA) with A from 10 to 18′. Absorbance was detected at 220 nm. The RCP of the (^{99m}Tc)-(CO)$_3$-SiNPs was determined by ascending instant thin layer chromatography with silica gel-coated fiberglass sheets (Pall Life Sciences, Pall Corporation, NY, USA) using physiological saline as the mobile phase.

In vitro uptake of radiolabeled SiNPs

SK-BR-3 (HER2$^+$) and MDA-MB-468 (HER2$^-$) cells were cultured at a density of 5×10^4 cells per well in 24-well plastic dishes (Corning) for 48 h. Cell plates were aspirated and 0.5 mL of DMEM supplemented with 10% FBS solution was added to each plate. Either ^{99m}Tc-labeled SiNP-NTA or SiNP-NTA-TZ suspensions (1 µCi/mL) were added to the plates in 0.5 mL volumes. The cells were then incubated at 37°C for 1, 4 and 24 h in a humidified atmosphere, 5% CO$_2$ air (three wells per condition). After specific periods, the DMEM NP suspensions was removed and the cells were washed with 300 µL of PBS. The PBS solution was removed and the cells were extracted using 200 µL of 0.05% Trypsin-EDTA (1×) solution for 10 min. The radioactivity of the cells and of each removed solution was then measured using a γ-counter (LKB Compugamma CS 1282). The percentage of radioactivity in cells over the total radioactivity for each plate was calculated.

Ex vivo biodistribution and fluorescence imaging of ^{99m}Tc-SiNPs in tumor

^{99m}Tc-labeled SiNPs were evaluated in two experimental groups of Balb/c nude mice. Mice in both groups were anesthetized with Zoletil (25 mg/kg of body weight) injected intraperitoneally, with additional supplemental anesthetic as needed. Two groups of 12 mice were injected in a tail vein with 100 µL of a solution containing ^{99m}Tc-labeled SiNP-NTA-TZ or ^{99m}Tc-labeled SiNP-NTA (1 mCi/mL, pH ~7.4).

Additional aliquots (0.1 mL) of both radioactive solutions were diluted 1:10, 1:100 and 1:1,000 and used to calculate the standard curve. Four animals per experimental point were sacrificed (at 4, 6 and 24 h, postinjection) under general anesthesia. Tumor and a sample of muscle were removed and placed in counting vials for counting and weighing. Tissue samples and standards were placed in a γ-counter and counts corrected for physical decay. The radioactivity concentration in tumor was calculated as percentage of injected dose per gram of tissue (% ID/g) and expressed as tumor to muscle ratio.

After counting, tumors obtained at 4 and 24 h postinjection were fixed with 4% paraformaldehyde for 3 h and embedded in Optimal Cutting Temperature compound mounting medium (Sakura Finetek, Torrance, CA, USA), to prepare frozen sections (10 µm). Sections were incubated with 4′,6-diamidino-2-phenylindole (DAPI) for 5 min, finally sealed with antifluorescence quenching agent (Beyotime, Sigma-Aldrich, Italy) and observed by fluorescence microscopy (Nikon Eclipse 80i). Samples collected at 4 h were also processed for β-actin immunofluorescent staining before DAPI labeling. In brief, tumor sections were rinsed with PBS and blocked with 5% BSA for 60 min, followed by incubation with primary antibody (rabbit anti-β-actin, diluted 1:50; Sigma-Aldrich) overnight at 4°C. The day after, tumor sections were washed for 5 min three times with PBS. Sections were then incubated with secondary antibody (Alexa Fluor488-labeled goat anti-rabbit IgG, diluted 1:200; Sigma-Aldrich) for 60 min at RT.

Results
Synthesis and characterization of SiNPs

Thanks to their versatility and robust chemistry, SiNPs are promising candidates to be used as nuclear medicine imaging probes.[28] In this study, monodisperse 50 nm spherical SiNPs were chosen as starting material to generate biocompatible multifunctional nanoconjugates. First, in order to have a fluorescent detectable carrier, the dense core of the SiNPs was loaded with a fluorophore, which was protected by an external denser silica shell necessary to prevent the undesired cargo release and limit the dye bleaching that often leads to misleading optical artifacts.[25] The uniform fluorescent core was obtained by a hydrolysis-condensation reaction of a mixture of TEOS and previously prepared APTMS-FITC complex[25] following a Stöber method in an ethanolic ammonia solution. A subsequent phase transfer to ultrapure water was followed by a biosilicification step catalyzed by L-arginine to create a uniform 5 nm-thick shell to further stabilize the fluorescent
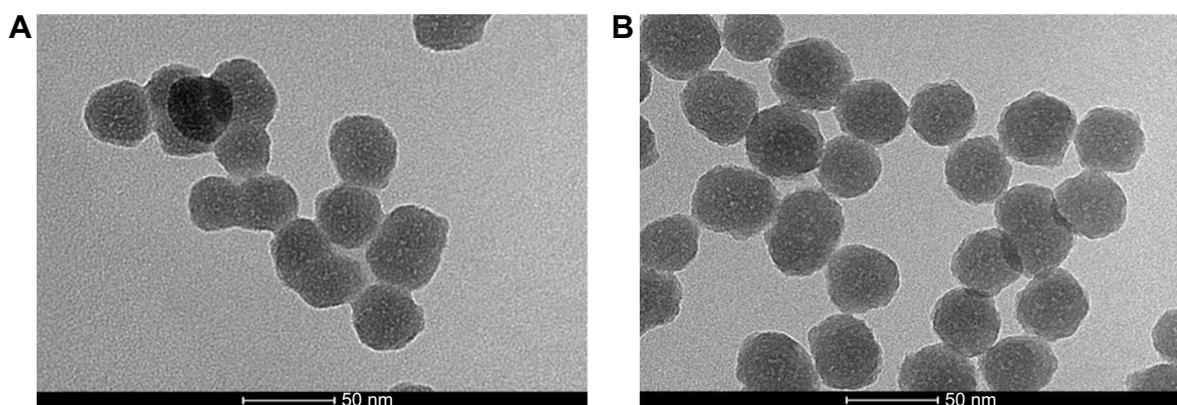
Figure 1 TEM images showing silica NPs before (**A**) and after (**B**) the shell synthesis.
Abbreviations: NPs, nanoparticles; TEM, transmission electron microscopy.

nanoconjugate (Figure 1).[29] The as-prepared core-shell SiNPs exhibited narrow size distribution and good colloidal stability in aqueous solution for months. After the NP fabrication, we optimized the functionalization steps with two main goals: 1) the introduction of a specific marker for the recognition of the HER2^{+} receptor in HER2^{+} cancer, and 2) the introduction of a radioisotope for SPECT imaging. The free silica surface was then engineered both to expose a targeting moiety and to host a proper chelating agent for radiolabeling. In particular, four types of silica nanoconjugates were synthesized and compared in order to evaluate the contribution of each functional moiety on the colloidal stability and on the fate of the resulting NPs (Table 1). Among the available radionuclides, we chose to introduce ^{99m}Tc as its 6 h half-life allowed us to follow the distribution of radiolabeled nanosilica in biological compartments. In addition, ^{99m}Tc nuclei emits only 140 keV characteristic γ-rays which, unlike β-rays that are usually emitted by other radionuclides, are absorbed far from the examined organ and minimize the danger posed to living matter. This property makes them highly desirable in nuclear medicine applications. In order to attach and retain the radionuclide, we decided to make use of the nitrilotriacetic acid chelating linker. A silane derivative (IPTES-NTA complex) was synthesized and grafted on the silica surface together with APTMS residues, thus introducing the chelating and amine functionalities in a one pot reaction (Scheme 1,

step 1). The NTA carboxylic moieties were then engaged in Ni^{2+} chelation before the radiolabeling steps. To achieve an active targeting of nanoconjugates toward HER2^{+} BC cells, Hc-TZ was considered an ideal ligand candidate, as it previously demonstrated to provide a prolonged accumulation of nanoconjugates in HER2^{+} breast tumors, compared to other molecular targeting agents, such as entire TZ or the relevant scFv fragment.[19] Therefore, a heterobifunctional PEG containing a maleimido group was covalently linked to the amine residues of the SiNPs (Scheme 1, step 2). After the reduction of disulfide bonds bridging the two chains of the antibody, the resulting thiol groups of the Hc-TZ were reacted with the maleimides, leading to the immobilization of the antibody on the shell surface (Scheme 1, step 3). Unreacted functional groups were saturated with a methoxyl terminating PEG. As a result, the whole nanoconjugate consisted of a fluorescent core-shell structure modified with multiple functionalities, including a chelating group, a targeting moiety and a biocompatible PEG coating. As stated before, the impact of each functionalization step was assessed by comparing the four synthetic silica nanoconjugates (SiNP, SiNP-TZ, SiNP-NTA and SiNP-NTA-TZ) differing from each other by the lack of one or more units. All the SiNP conjugates were characterized in terms of hydrodynamic size and ζ-potential (Table 1). SiNP and SiNP-TZ showed a hydrodynamic diameter (Hd) <100 nm with good polydispersity indexes (<0.120).

Table 1 Properties of nanoconjugates evaluated in this study

| Nanoconjugate	Functionalization	Hydrodynamic size (nm)	PDI	ζ-potential (mV)
SiNP	Only PEG	85.59±9.49	0.119±0.091	−30.2±0.30
SiNP-TZ	PEG + TZ	93.61±6.22	0.095±0.027	−31.6±0.30
SiNP-NTA	PEG + NTA	123.9±29.77	0.114±0.024	−33.5±6.55
SiNP-NTA-TZ	PEG + NTA + TZ	114.3±0.70	0.084±0.001	−33.6±6.00

Note: Data are the mean ± standard deviation of three different NP batches.
Abbreviations: NP, nanoparticle; PDI, polydispersity index; PEG, polyethylene glycol; TZ, trastuzumab; NTA, nitrilotriacetic acid.
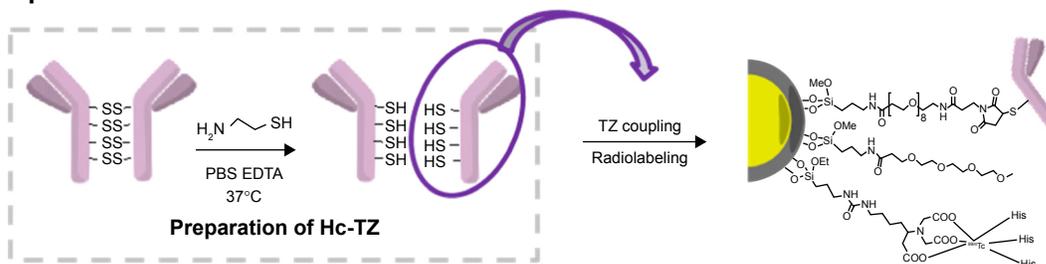
Step 1
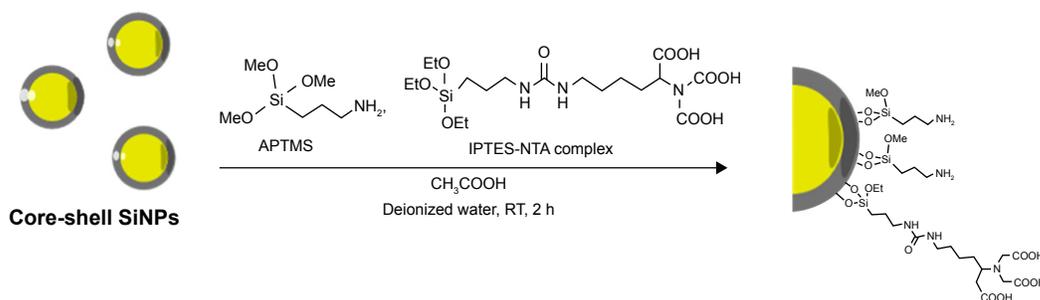
Step 2
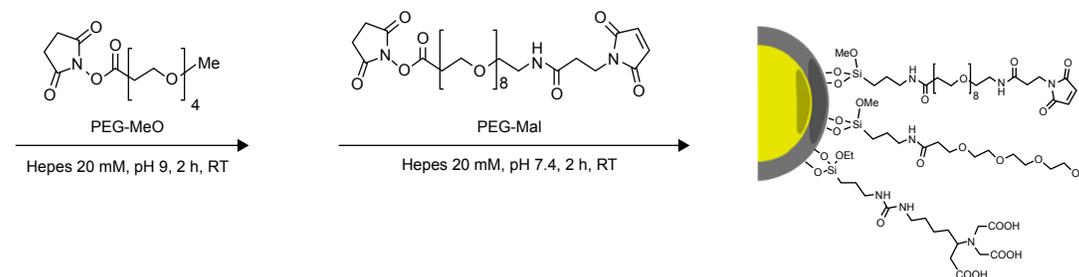
Step 3

Scheme 1 Schematic representation of the synthetic steps for the preparation of SiNP-NTA-TZ.
Abbreviations: TZ, trastuzumab; PBS, phosphate saline buffer; RT, room temperature.

In contrast, the presence of the NTA linker, especially upon Ni^{2+} ion chelation, led to a mild aggregation for SiNP-NTA and SiNP-NTA-TZ (Hd >100 nm), which however was limited by the radiolabeling procedure. The characteristic negative ζ-potential of the SiNPs was maintained for all kinds of nanoconjugates, which is an important prerequisite for low toxicity and systemic diffusion in vivo.[30] TZ presence on SiNP surface was confirmed by Dot Blot analysis. SiNP-TZ showed a clear signal compared to SiNP and core-shell NPs used as negative control (Figure S1).

In vitro binding efficiency and selectivity of SiNPs by flow cytometry

Binding selectivity of SiNPs toward HER2+ BC cells was first evaluated by flow cytometry. To validate this system, SK-BR-3 cells were chosen as HER2+ BC model, whereas HER2-negative (HER2−) MDA-MB-468 cells were used as negative control. To investigate the impact of functionalization

on the binding capacity of SiNPs, the study was performed comparing SiNP vs SiNP-TZ and SiNP-NTA vs SiNP-NTA-TZ (Figure 2). Each kind of nanoconjugate was separately incubated for different time periods (20 min, 1 h, 4 h and 24 h) in SK-BR-3 cells (Figure S2) and MDA-MB-468 cells (Figure S3). Flow cytometry evidenced a remarkable time-dependent increase of fluorescence signal after incubation of SiNP-TZ/SiNP-NTA-TZ with SK-BR-3 cells (Figure 2B and D), and a significant difference ($P<0.05$) compared to MDA-MB-468 cells. This data demonstrated the capability of targeted NPs to selectively recognize HER2 receptors in SK-BR-3 cells. SiNP/SiNP-NTA exhibited a remarkably lower uptake in SK-BR-3 cells compared to Hc-TZ-modified SiNPs and no preferential affinity toward SK-BR-3 or MDA-MB-468 cell lines was found (Figure 2A and C), suggesting that the interaction with cells was essentially attributable to nonspecific uptake in both HER2− or HER2+ cells. However, nonspecific uptake was basically negligible within the first 4 h.
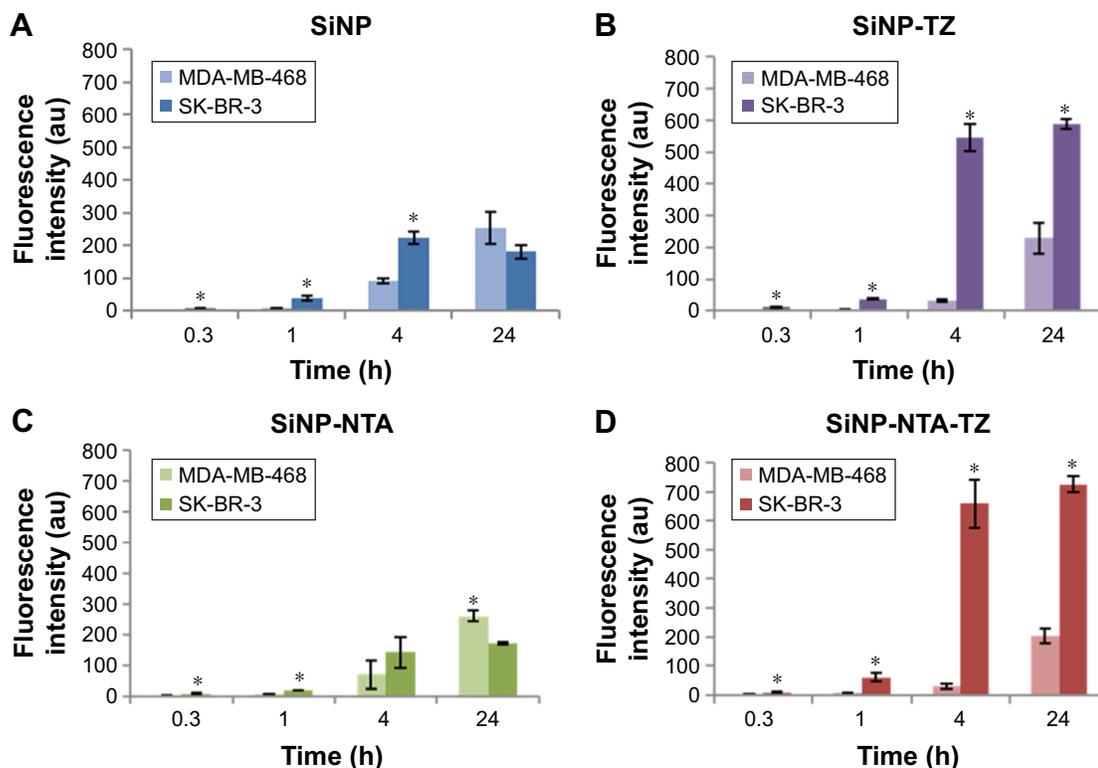
Figure 2 Assessment of nanoparticle–cell interaction by flow cytometry.
Note: Panels (**A–D**) represent the distribution of cell fluorescence intensity, normalized over untreated cells (control), in MDA-MB-468 and SK-BR-3 cell lines after exposure to (**A**) SiNP, (**B**) SiNP-TZ, (**C**) SiNP-NTA and (**D**) SiNP-NTA-TZ at 20 min, 1 h, 4 h and 24 h at a concentration of 50 mg/mL (Student's t-test; *$P < 0.05$ vs MDA-MB-468).
Abbreviations: NP, nanoparticle; TZ, trastuzumab; NTA, nitrilotriacetic acid.

In vitro fluorescence imaging

To validate the flow cytometry data, the binding specificity of Hc-TZ-modified SiNPs for HER2+ cells was assessed by fluorescence microscopy (Figure 3). Images of SiNPs (green) were overlaid on the corresponding nuclei image counterstained with Hoechst solution. SiNP, SiNP-TZ, SiNP-NTA and SiNP-NTA-TZ were incubated in parallel in SK-BR-3 and MDA-MB-468 cells for 20 min, 1 h, 4 h and 24 h. Fluorescence microscopy images showed that green fluorescence signal started to increase in HER2+ cells after 1 h of incubation with SiNP-NTA-TZ. In these cells, fluorescence intensity increased over time and was considerably stronger than that shown in SiNP-NTA images. We did not observe any differences in the behavior of SiNP-TZ and SiNP-NTA-TZ (Figure S4). In addition, SiNP-NTA fluorescence intensity showed no significant difference in both cell lines, confirming the loss of selectivity for SiNPs in the absence of Hc-TZ conjugation. SK-BR-3 pictures acquired at 4 and 24 h exhibited a perinuclear localization of green fluorescence signals exclusively after incubation with SiNP-NTA-TZ. In contrast, SiNP-NTA-TZ signal was not found in the cytoplasm of HER2− cells and remained localized outside the cells after 4 and 24 h of incubation. At these time points,

it was apparent that a large number of SiNP-NTA-TZ was internalized by HER2+ SK-BR-3 cells, different from HER2+ cells, the NPs are taken up to a much lower extent in HER2− cells MDA-MB-468 cells, confirming the specific targeting of Hc-TZ-functionalized SiNPs for HER2+ tumor cells.

NPs toxicity

Cell toxicity of all SiNPs was assessed in HER2+ SK-BR-3 and HER2− MDA-MB-468 BC cells. First, we evaluated the effects of SiNP, SiNP-TZ, SiNP-NTA and SiNP-NTA-TZ on mitochondrial metabolism through MTT assay performed at 1, 4, 24 and 48 h of incubation with a solution of SiNPs (100 μg/mL). The analysis (MTT test) showed no relevant toxic effect on both cell lines (Figure 4A) compared to untreated samples. Viability values higher than 100% are related to changes in rate of endo-/exocytosis and intracellular trafficking of MTT-formazan, which may interfere with MTT reduction. This effect, that does not interfere with the cell viability or Trypan blue assay, was already observed by others.[31]

Viability (cell counting) of SK-BR-3 and MDA-MB-468 cells exposed to the NPs was also investigated. Cell proliferation in both cell lines was not significantly affected after 1, 4, 24 and 48 h of exposure with all sets of NPs (Figure 4B).
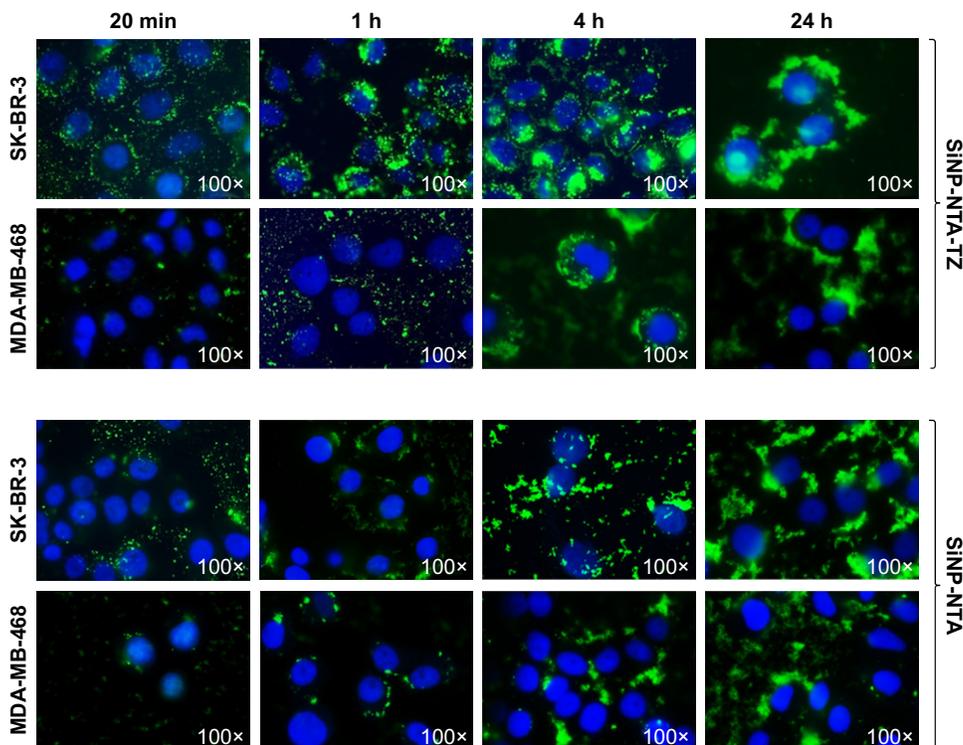
Figure 3 Specificity binding by fluorescence microscopy.
Notes: SK-BR-3 and MDA-MB-468 cells were grown on coverslips for 24 h and then exposed for 20 min, 1, 4 and 24 h to 50 µg/mL of FITC-labeled (green) SiNPs functionalized with (SiNP-NTA-TZ) or without (SiNP-NTA) Hc-TZ. Nuclei were stained with Hoechst (blue).
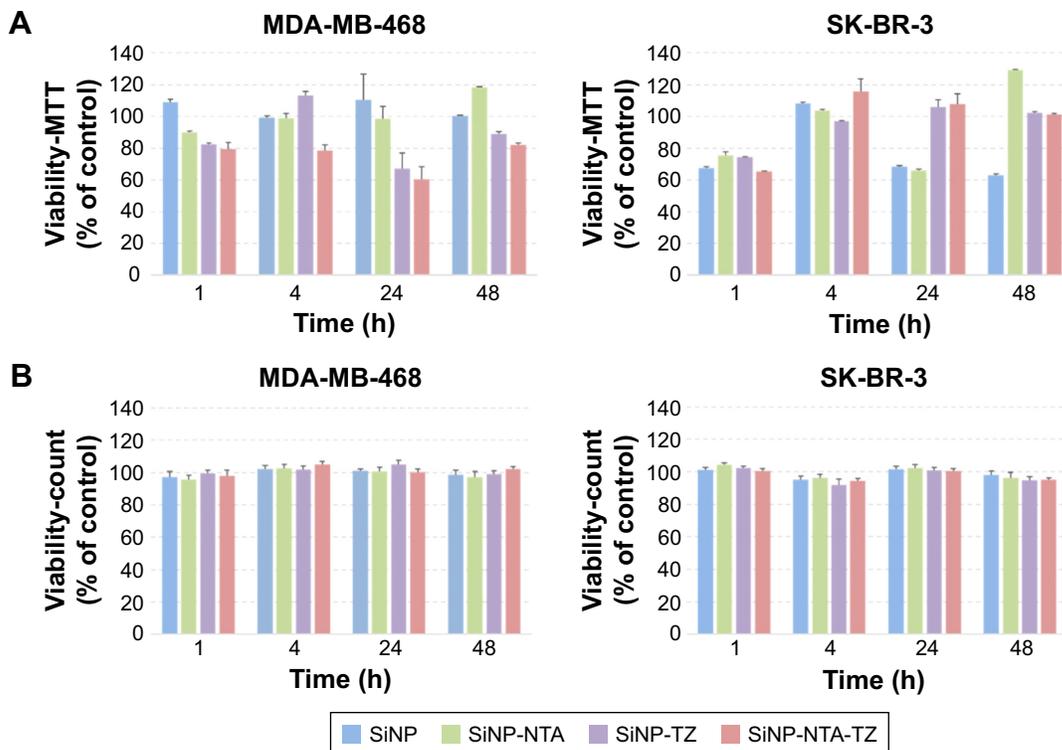**Abbreviations:** FITC, fluorescein isothiocyanate; NP, nanoparticle; TZ, trastuzumab; NTA, nitrilotriacetic acid.

Figure 4 SiNPs toxicity was investigated both by (**A**) MTT and (**B**) cell viability tests.
Notes: SK-BR-3, MDA-MB-468 cells were incubated with SiNPs (100 µg/mL) for 1, 4, 24 and 48 h. Survival rate threshold of 60%.
Abbreviations: NP, nanoparticle; TZ, trastuzumab; NTA, nitrilotriacetic acid.

MTT test was replicated at 4 and 24 h in nontransformed mammary epithelial MCF-10A cell line (HER2$^-$) and confirmed the absence of cytotoxic effect caused by the NPs (Figure S5). Taken together, these results indicated a good profile of safety for all nanoconstructs in cultures of both tumor and healthy mammary cells.

SiNPs radiolabeling with ^{99m}Tc

The tricarbonyl method developed by Waibel et al,[32] offers a convenient solution to label proteins with ^{99m}Tc radionuclide, enabling labeling without prior modification with bifunctional chelators. The $(^{99m}Tc[CO]_3[OH_2]_3)^+$ is an excellent precursor for ^{99m}Tc labeling of biomolecules, being stable and substitution-reactive.[33] This precursor is highly water-soluble and reveals good stability in aqueous solution over a broad pH range (pH 2–12) for several hours. The three coordinated water molecules are promptly substituted by a variety of functional groups, including amines, thioethers, thiols and phosphines. The RCP of ^{99m}Tc(I) tricarbonyl ion solution could be easily checked by TLC and HPLC. The ^{99m}Tc(I) tricarbonyl ion was then introduced using a new approach, involving three steps: 1) prelabeling of ^{99m}Tc–tricarbonyl core, 2) reaction with poly-His peptide, 3) conjugation to NTA groups of SiNP-NTA and SiNP-NTA-TZ.[34] With this approach, SiNPs were functionalized with 4 nmol NTA per mg of NPs, while the molar ratio between NTA and poly-His was 1:3. The reaction between tricarbonyl precursor and hexa-His-Tag peptide was almost quantitative (Figure S6). The stability of $(^{99m}Tc[CO]_3)^+$-His was checked after 24 h (Figure S7).

In vitro uptake of radiolabeled ^{99m}Tc-SiNPs

To assess the selectivity of ^{99m}Tc-labeled NPs toward HER2$^+$ cells, we tested NTA-nanoconstructs with or without Hc-TZ in a kinetic binding assay on HER2$^+$ SK-BR-3 in comparison to HER2$^-$ MDA-MB-468 cells. ^{99m}Tc-labeled SiNP-NTA and SiNP-NTA-TZ were incubated in both cell lines at 1, 4 and 24 h. At these time points, media were removed and counted using a γ-counter and cells washed, removed and counted to calculate NPs uptake as % of total radioactivity administered. Specific binding curves were generated as shown in Figure 5. SiNP-NTA was bound weakly and nonspecifically to both the MDA-MB-468 and the SK-BR-3 cells, giving a maximum value of 1.4% uptake 24 h after incubation (Figure 5A). In contrast, SiNP-NTA-TZ had already shown an uptake value of 1.6% in SK-BR-3 cells after 1 h of incubation, reaching 2.3% at 4 h, compared to 1.1% of uptake observed in MDA-MB-468 cells ($P<0.05$). It is apparent that the specific uptake ratio (SK-BR-3/MDA-MB-468) for SiNP-NTA-TZ was maximum at this time point. The uptake of SiNP-NTA-TZ continued to increase up to 24 h showing a slight increase in both cell lines, following a similar nonspecific trend, and reaching an uptake value of 3.7% in HER2$^+$ cells and 2.1% in HER2$^-$ cells (Figure 5B).

Ex vivo biodistribution and fluorescence imaging of ^{99m}Tc-SiNPs in tumor

Biodistribution pattern of ^{99m}Tc-labeled NPs (SiNP-NTA and SiNP-NTA-TZ) was assessed in a SK-BR-3 tumor mouse model at 4, 6 and 24 h. Results are summarized in Figure 6.
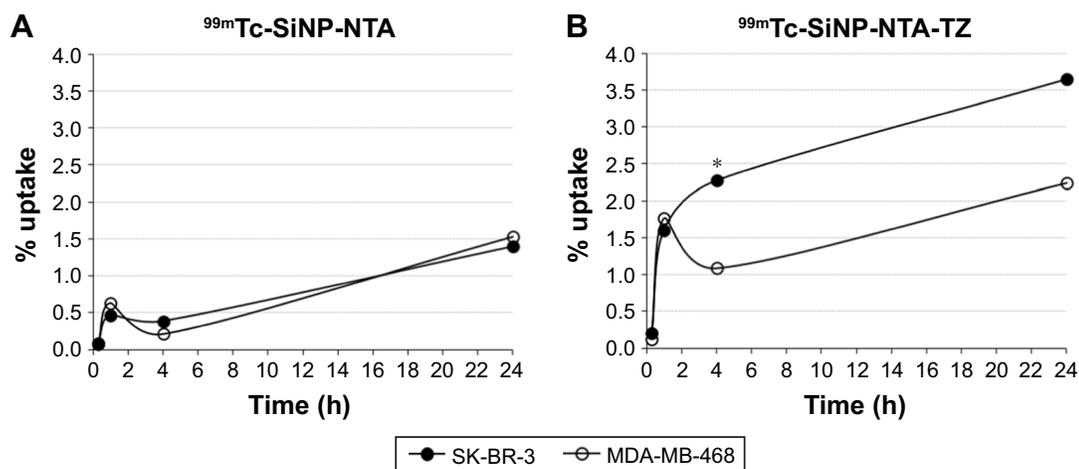

Figure 5 In vitro uptake of ^{99m}Tc-radiolabeled (**A**) SiNP-NTA and (**B**) SiNP-NTA-TZ NPs.
Notes: SK-BR-3 and MDA-MB-468 cells were incubated with SiNPs (1 μCi/mL) for 1, 4 and 24 h. Cell uptake was expressed as % of total radioactivity administered (Student's *t*-test; *$P<0.05$ vs MDA-MB-468).
Abbreviations: NP, nanoparticle; TZ, trastuzumab; NTA, nitrilotriacetic acid.
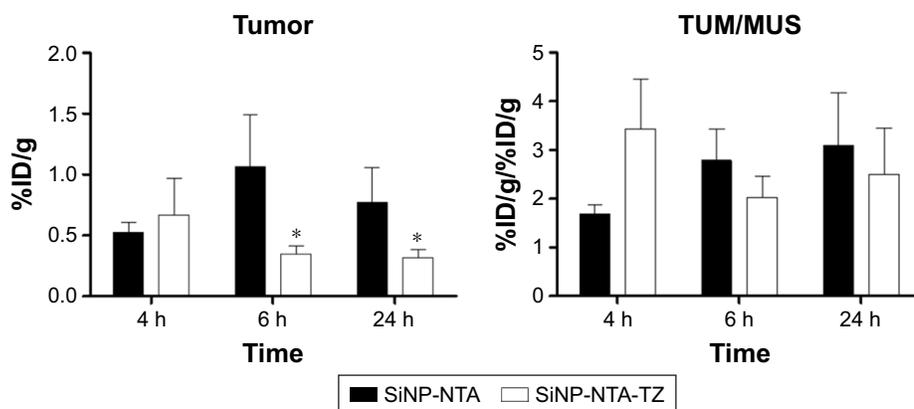
Figure 6 Ex vivo biodistribution of ^{99m}Tc-labeled SiNP-NTA and SiNP-NTA-TZ nanoparticles in HER$^+$ breast cancer model.
Notes: SK-BR-3 tumor bearing mice were sacrificed at 4, 6 h (n=3) and 24 h (n=4) postinjection. Samples were dissected and analyzed by γ-counter to obtain tumor-to-muscle ratio (on the right) of %ID/g (on the left) values. Statistical differences between SiNP-NTA and SiNP-NTA-TZ were evaluated by Student's t-test; *$P<0.05$.
Abbreviations: NP, nanoparticle; TZ, trastuzumab; NTA, nitrilotriacetic acid; TUM/MUS, tumour/muscle.

At 4 h after injection of radiolabeled SiNP-NTA-TZ or SiNP-NTA, radioactivity accumulation in SK-BR-3 tumor was higher for TZ-conjugated NPs compared to nonconjugated NPs. At this time, mean tumor uptake (expressed as % ID/g) was 0.52±0.08 for SiNP-NTA and 0.67±0.03 for SiNP-NTA-TZ, and tumor-to-muscle ratios of % ID/g were 1.69±0.18 and 3.45±1.02 for SiNP-NTA and SiNP-NTA-TZ, respectively. At longer times of exposure, we observed a reduction in tumor radioactivity concentration for animals injected with SiNP-NTA-TZ but not in those injected with SiNP-NTA ($P<0.05$ at 6 and 24 h). The decline of SiNP-NTA-TZ uptake value, observed from 6 h postinjection, could be explained by an active targeting followed by lysosomal degradation and consequent clearance of NP shell labeled with ^{99m}Tc. The higher radioactivity uptake observed in animals injected with SiNP-NTA suggests passive targeting promoted by tumor EPR effect. Considering the other organs, high levels of radioactivity were observed for both NPs in liver, kidney and spleen, even with different kinetics (Table S1). To better understand the ex vivo tumor uptake data obtained by radioactivity counting, the targeting specificity of ^{99m}Tc-labeled NPs (SiNP-NTA-TZ vs SiNP-NTA) in SK-BR-3 lesions was assessed by postmortem fluorescence microscopy. Immunofluorescence staining of tumor cryosections collected at 4 and 24 h postinjection allowed us to establish the distribution of the two nanotracers (Figures 7 and S8). Images of SiNPs (green) and β-actin (red) were overlaid on the corresponding images reporting nuclei (blue). Fluorescence intensity in SiNP-NTA-TZ images was significantly higher than that observed for SiNP-NTA and it was mainly localized in the perinuclear area. In contrast, green fluorescence distribution in SiNP-NTA images was
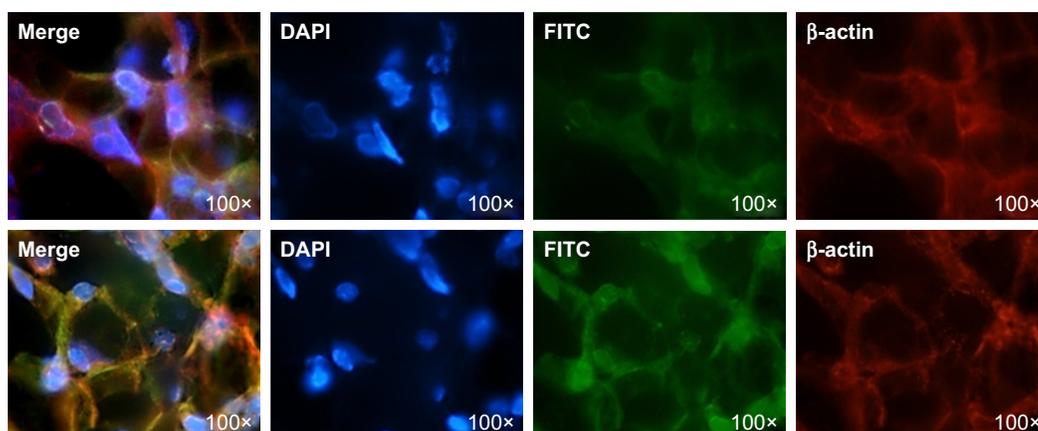

Figure 7 Ex vivo immunofluorescence of SK-BR-3 tumor cryosections collected at 4 h postinjection of SiNP-NTA (top) and SiNP-NTA-TZ (bottom).
Note: Merge images represent the colocalization of SiNPs (green), β-actin (red) and reporting nuclei (blue).
Abbreviations: DAPI, 4′,6-diamidino-2-phenylindole; FITC, fluorescein isothiocyanate; NP, nanoparticle; TZ, trastuzumab.

barely detectable on the surface of SK-BR-3 tumor cell membrane. Fluorescence signal was still present at 24 h postinjection ([Figure S8](#)).

Discussion

HER2 is the product of a proto-oncogene and its overexpression was firstly observed in BC and is associated with malignant tumor phenotype, with poorer prognosis related to the degree of expression.[35] At present, the detection of HER2 in BC and in its metastases is based on invasive methods, such as biopsy, to obtain representative tissue for IHC phenotyping.[36] Recently, new approaches were developed to determine soluble markers such as HER2 extracellular domain and circulating miRNA for patients' stratification, but these strategies have not been standardized yet.[37,38] To overcome the current limitation, a series of radiopharmaceuticals assembled with antibodies, nanobodies or affibodies have been developed and some of these are already under clinical evaluation for use as PET or SPECT nuclear imaging agents for in vivo molecular detection of HER2 receptor.[39,40] This study describes the use of a multifunctional NP system, able to act as a SPECT radiotracer for tumor detection and opening the opportunity to develop a new generation of theranostic nanoagents to be used for noninvasive detection of HER2^{+} cells and targeted drug delivery.[41,42] In fact, although chemotherapy in combination with TZ administration has been reported to play an important role in the treatment of HER2^{+} BC, about 70% of patients demonstrated resistance.[43] The use of nontargeted chemotherapeutic drugs significantly limits the drug accumulation within cancer cells and induces undesired toxic side effects toward normal tissues.[44] In this context, radiolabeled silica nanocarriers could represent a significant advance in the identification and treatment of HER2^{+} BC lesions. To this aim, we designed and tested ^{99m}Tc-radiolabeled SiNPs for the selective detection of HER2 receptor in malignant BC cells, capitalizing on Hc-TZ functionalization. Our results suggest that receptor-mediated active targeting provided the best efficiency in BC detection, compared to simple EPR passive accumulation. We evaluated the behavior and the targeting efficiency of SiNPs functionalized or not with Hc-TZ, in BC models in in vitro and ex vivo experiments, before and after radiolabeling. In vitro, flow cytometry data showed a remarkable increase in uptake over time after incubation of SiNP-TZ/SiNP-NTA-TZ with HER2^{+} SK-BR-3 cells, compared to SiNP/SiNP-NTA. As expected, the uptake of all SiNPs tested remained low in HER2^{−} MDA-MB-468 cells. These results were confirmed by fluorescence microscopy, which exhibited a considerable

perinuclear localization in SK-BR-3 cells exclusively upon incubation with SiNP-TZ/SiNP-NTA-TZ, while an external localization of fluorescence signal was observed in MDA-MB-468 cells with both SiNP-TZ/SiNP-NTA-TZ and SiNP/SiNP-NTA. In vitro toxicity assay of each SiNP set did not reveal significant impact on mitochondrial metabolism and cell viability in HER2^{+}/HER^{−} malignant cells and in nontransformed mammary epithelial cells. The high efficiency and selectivity of Hc-TZ-modified SiNPs in the recognition of HER2^{+} cells were also assessed after radiolabeling. Well established protocols to radiolabel antibodies are reported in the literature.[45] However, we preferred to develop a new approach based on immobilization of radioligand to the NP surface obtaining a radiolabeled nanoscaffold common to the different nanoconstructs synthesized within this study, independent from the functionalization with the antibody chain. Radiolabeling of both SiNP-NTA and SiNP-NTA-TZ was achieved by formation of radioligand-NTA complex. The in vitro uptake of ^{99m}Tc-SiNPs in HER2^{+}/HER^{−} cells confirmed the results from flow cytometry, suggesting that our radiolabeling strategy did not affect the nanoconjugate binding capability. Next, the radiolabeled SiNPs efficiency in detecting HER2^{+} cells was also evaluated in a SK-BR-3 xenograft animal model. Ex vivo biodistribution of ^{99m}Tc-SiNP-NTA-TZ showed a preferential tumor distribution at 4 h postinjection compared to ^{99m}Tc-SiNP-NTA, confirming the involvement of Hc-TZ moiety in the targeting efficiency of the nanoconstruct compared to EPR passive accumulation. The drop of SiNP-NTA-TZ uptake value at late time points may represent a further potential confirmation of an active targeting mechanism, involving receptor-mediated endocytosis, which leads to lysosomal (pH≈4–5) degradation of radiolabeled nanocomplex with time, as previously described with different colloidal NPs.[46] The labeling of NTA ligand (SiNP surface) with the ^{99m}Tc-tricarbonyl precursor, preserves its high stability in a physiological solution (pH≈7), while low pH condition may impair the property of this complex. In this condition, the destabilization of complex could promote the washout of radioactivity, due to ^{99m}Tc-tricarbonyl clearance instead to a real elimination of NPs core (FITC/Treatment). Indeed, fluorescence microscopy on HER[+] tumor cryosections confirmed for SiNP-NTA-TZ, at 4 and 24 h, a higher specificity of targeting compared to untargeted NPs, and a long circulation of their associated fluorescence signal, corroborating the possible use of this system as carrier for tumor therapy. In a recent study by Chen et al, mesoporous SiNPs were functionalized with the murine/human antibody TRC105 and used to target 4T1 BC

lesion in mice.[47] Tumor uptake of TRC105-conjugated NPs reached the maximum signal intensity at 5 h postinjection and was twofold higher compared to muscle (background) and to nonconjugated NPs used as controls. Those data were comparable with the results of our ex vivo uptake studies, in which we assessed the targeting efficiency of radiolabeled antibody-functionalized SiNP-NTA-TZ and nonfunctionalized SiNP-NTA. In addition, ^{99m}Tc-SiNP-NTA-TZ specific intracellular localization at 4 h was shown in vitro and postmortem by fluorescence imaging experiments, compared to ^{99m}Tc-SiNP-NTA. This mechanism was already described in SK-BR-3 cells using different NPs functionalized with TZ.[48,49] A similar strategy of ^{99m}Tc-labeling was described by Yamaguchi et al.[41] In this case, SiNPs were targeted with double chain anti-HER2 antibody, and at 4 h after injection, the authors observed higher levels of radioactivity uptake in SK-BR-3 tumor in comparison to HER2^{−}. However, despite the lower diameter of the NPs used in their study, tumor uptake values were inferior to that observed using our method of radiolabeling and particles platform, functionalized with TZ half-chain. The experimental data collected and the versatility of this NP-based system could be the basis for exploring new functionalization/radiolabeling strategies and for the possibility to load different dyes, for combined multimodal imaging. In addition, taking advantage of the easy and straightforward chemical functionalization of their surface with a plethora of functional ligands, several different kinds of therapeutics can be loaded to increase the efficiency and selectivity of nanoconjugates in order to improve patient stratification. In future studies, we will explore the possibility to directly introduce a radioisotope on the antibody chain (Hc-TZ) of SiNP-TZ, in order to follow the fate of the nanoconjugate components separately.

Conclusion

In summary, we have reported here an SiNP-based system for noninvasive detection, staging and potential treatment of HER2^{+} BC. Our radiolabeled system not only exhibited an enhanced targeting for the tumor, compared to EPR passive diffusion, but also significantly increased the selective accumulation of SiNPs within the HER2^{+} SK-BR-3 cells, taking advantage of an optimized conjugation to the half-chain fragment of the humanized antibody TZ, already in use in clinical practice. Our results are encouraging, suggesting further assessment of silica-radionuclide nanoconjugates with the aim to develop a new generation of versatile nanoreporters for enhanced-resolution nuclear medicine and to promote this system as a theranostic agent of highly aggressive HER2^{+} BC detection and treatment.

Author contributions

All authors contributed toward data analysis, drafting and revising the paper and agree to be accountable for all aspects of the work.

Disclosure

The authors report no conflicts of interest in this work.

References

1. Siegel RL, Miller KD, Jemal A. Cancer statistics, 2015. *CA Cancer J Clin*. 2015;65(1):5–29.
2. Slamon DJ, Leyland-Jones B, Shak S, et al. Use of chemotherapy plus a monoclonal antibody against HER2 for metastatic breast cancer that overexpresses HER2. *N Engl J Med*. 2001;344(11):783–792.
3. Chang HR. Trastuzumab-based neoadjuvant therapy in patients with HER2-positive breast cancer. *Cancer*. 2010;116(12):2856–2867.
4. Murthy RK, Varma A, Mishra P, et al. Effect of adjuvant/neoadjuvant trastuzumab on clinical outcomes in patients with HER2-positive metastatic breast cancer. *Cancer*. 2014;120(13):1932–1938.
5. Perez EA, Cortes J, Gonzalez-Angulo AM, Bartlett JM. HER2 testing: current status and future directions. *Cancer Treat Rev*. 2014;40(2): 276–284.
6. Gainkam LO, Huang L, Caveliers V, et al. Comparison of the biodistribution and tumor targeting of two 99mTc-labeled anti-EGFR nanobodies in mice, using pinhole SPECT/micro-CT. *J Nucl Med*. 2008;49(5): 788–795.
7. Jeraj R, Bradshaw T, Simoncic U. Molecular imaging to plan radiotherapy and evaluate its efficacy. *J Nucl Med*. 2015;56(11):1752–1765.
8. Ahlgren S, Wallberg H, Tran TA, et al. Targeting of HER2-expressing tumors with a site-specifically 99mTc-labeled recombinant affibody molecule, ZHER2:2395, with C-terminally engineered cysteine. *J Nucl Med*. 2009;50(5):781–789.
9. Meszaros LK, Dose A, Biagini SCG, Blower PJ. Hydrazinonicotinic acid (HYNIC) – Coordination chemistry and applications in radiopharmaceutical chemistry. *Inorg Chim Acta*. 2010;363(6):1059–1069.
10. Lipowska M, Marzilli LG, Taylor AT. Tc-99m(CO)(3)-Nitrilotriacetic Acid: a new renal radiopharmaceutical showing pharmacokinetic properties in rats comparable to those of I-131-OIH. *J Nucl Med*. 2009; 50(3):454–460.
11. Sobral DV, Miranda ACC, Barboza MF, Marques FLN, Nakaie CR, Malavolta L. Synthesis and characterization of 99mTc-Labeled peptides as a potential amyloid plaques imaging agent. *Biopolymers*. 2013;100(3): 295–295.
12. Lim EK, Kim T, Paik S, Haam S, Huh YM, Lee K. Nanomaterials for theranostics: recent advances and future challenges. *Chem Rev*. 2015; 115(1):327–394.
13. Orza A, Casciano D, Biris A. Nanomaterials for targeted drug delivery to cancer stem cells. *Drug Metab Rev*. 2014;46(2):191–206.
14. Bourzac K. Nanotechnology carrying drugs. *Nature*. 2012;491(7425): S58–S60.
15. Choi HS, Frangioni JV. Nanoparticles for biomedical imaging: fundamentals of clinical translation. *Mol Imaging*. 2010;9(6):291–310.
16. Maeda H, Wu J, Sawa T, Matsumura Y, Hori K. Tumor vascular permeability and the EPR effect in macromolecular therapeutics: a review. *J Control Release*. 2000;65(1–2):271–284.

17. Bertrand N, Wu J, Xu XY, Kamaly N, Farokhzad OC. Cancer nanotechnology: the impact of passive and active targeting in the era of modern cancer biology. *Adv Drug Deliver Rev*. 2014;66:2–25.

18. Baselga J, Swain SM. Novel anticancer targets: revisiting ERBB2 and discovering ERBB3. *Nature Reviews Cancer*. 2009;9(7):463–475.

19. Fiandra L, Mazzucchelli S, De Palma C, et al. Assessing the in vivo targeting efficiency of multifunctional nanoconstructs bearing antibody-derived ligands. *ACS Nano*. 2013;7(7):6092–6102.

20. Chow EKH, Ho D. Cancer nanomedicine: from drug delivery to imaging. *Sci Transl Med*. 2013;5(216):216rv4.

21. Vivero-Escoto JL, Huxford-Phillips RC, Lin WB. Silica-based nanoprobes for biomedical imaging and theranostic applications. *Chem Soc Rev*. 2012;41(7):2673–2685.

22. Benezra M, Penate-Medina O, Zanzonico PB, et al. Multimodal silica nanoparticles are effective cancer-targeted probes in a model of human melanoma. *J Clin Invest*. 2011;121(7):2768–2780.

23. Kempen PJ, Greasley S, Parker KA, et al. Theranostic mesoporous silica nanoparticles biodegrade after pro-survival drug delivery and ultrasound/magnetic resonance imaging of stem cells. *Theranostics*. 2015;5(6):631–642.

24. Veeranarayanan S, Poulose AC, Mohamed MS, et al. Synergistic targeting of cancer and associated angiogenesis using triple-targeted dual-drug silica nanoformulations for theragnostics. *Small*. 2012;8(22):3476–3489.

25. Mahon E, Hristov DR, Dawson KA. Stabilising fluorescent silica nanoparticles against dissolution effects for biological studies. *Chem Commun (Camb)*. 2012;48(64):7970–7972.

26. Soto-Cantu E, Cueto R, Koch J, Russo PS. Synthesis and rapid characterization of amine-functionalized silica. *Langmuir*. 2012;28(13):5562–5569.

27. Almutary A, Sanderson BJ. The MTT and crystal violet assays: Potential confounders in nanoparticle toxicity testing. *Int J Toxicol*. 2016;35(4):454–462.

28. Bae SW, Tan WH, Hong JI. Fluorescent dye-doped silica nanoparticles: new tools for bioapplications. *Chem Commun (Camb)*. 2012;48(17):2270–2282.

29. Yokoi T, Sakamoto Y, Terasaki O, Kubota Y, Okubo T, Tatsumi T. Periodic arrangement of silica nanospheres assisted by amino acids. *J Am Chem Soc*. 2006;128(42):13664–13665.

30. Blanco E, Shen H, Ferrari M. Principles of nanoparticle design for overcoming biological barriers to drug delivery. *Nat Biotechnol*. 2015;33(9):941–951.

31. Stepanenko AA, Dmitrenko VV. Pitfalls of the MTT assay: direct and off-target effects of inhibitors can result in over/underestimation of cell viability. *Gene*. 2015;574(2):193–203.

32. Waibel R, Alberto R, Willuda J, et al. Stable one-step technetium-99m labeling of His-tagged recombinant proteins with a novel Tc(I)-carbonyl complex. *Nat Biotechnol*. 1999;17(9):897–901.

33. Alberto R, Schibli R, Egli A, Schubiger AP, Abram U, Kaden TA. A novel organometallic aqua complex of technetium for the labeling of biomolecules: Synthesis of [Tc-99m(OH2)(3)(CO)(3)](+) from [(TcO4)-Tc-99m](-) in aqueous solution and its reaction with a bifunctional ligand. *J Am Chem Soc*. 1998;120(31):7987–7988.

34. Badar A, Williams J, de Rosales RTM, et al. Optimising the radiolabelling properties of technetium tricarbonyl and His-tagged proteins. *EJNMMI Res*. 2014;4(1):14.

35. Couto Mdo R, Pinto D, Oliveira J, et al. [The predictive and monitoring value of serum HER2/NEU in breast cancer under trastuzumab therapy.] *Acta Med Port*. 2011;24(1):5–16. Portuguese.

36. Gutierrez C, Schiff R. HER2: biology, detection, and clinical implications. *Arch Pathol Lab Med*. 2011;135(1):55–62.

37. Leyland-Jones B, Smith BR. Serum HER2 testing in patients with HER2-positive breast cancer: the death knell tolls. *Lancet Oncol*. 2011;12(3):286–295.

38. Graveel CR, Calderone HM, Westerhuis JJ, Winn ME, Sempere LF. Critical analysis of the potential for microRNA biomarkers in breast cancer management. *Breast Cancer*. 2015;7:59–79.

39. Vaidyanathan G, McDougald D, Choi J, et al. Preclinical evaluation of 18F-Labeled anti-HER2 nanobody conjugates for imaging HER2 receptor expression by immuno-PET. *J Nucl Med*. 2016;57(6):967–973.

40. Xavier C, Blykers A, Vaneycken I, et al. (18)F-nanobody for PET imaging of HER2 overexpressing tumors. *Nucl Med Biol*. 2016;43(4):247–252.

41. Yamaguchi H, Tsuchimochi M, Hayama K, Kawase T, Tsubokawa N. Dual-labeled near-infrared/(99m)Tc imaging probes using PAMAM-coated silica nanoparticles for the imaging of HER2-expressing cancer cells. *Int J Mol Sci*. 2016;17(7)1086.

42. Geng J, Liu J, Liang J, Shi H, Liu B. A general approach to prepare conjugated polymer dot embedded silica nanoparticles with a SiO2@CP@SiO2 structure for targeted HER2-positive cellular imaging. *Nanoscale*. 2013;5(18):8593–8601.

43. Pohlmann PR, Mayer IA, Mernaugh R. Resistance to trastuzumab in breast cancer. *Clin Cancer Res*. 2009;15(24):7479–7491.

44. Ma B, Ma QQ, Wang HQ, Zhang GL, Zhang HY, Wang XH. Clinical efficacy and safety of T-DM1 for patients with HER2-positive breast cancer. *Onco Targets Ther*. 2016;9:959–976.

45. Li C, Zhang Y, Wang L, et al. A novel multivalent (99m)Tc-labeled EG2-C4bpalpha antibody for targeting the epidermal growth factor receptor in tumor xenografts. *Nucl Med Biol*. 2015;42(6):547–554.

46. Corsi F, Fiandra L, De Palma C, et al. HER2 expression in breast cancer cells is downregulated upon active targeting by antibody-engineered multifunctional nanoparticles in mice. *ACS Nano*. 2011;5(8):6383–6393.

47. Chen F, Nayak TR, Goel S, et al. In vivo tumor vasculature targeted PET/NIRF imaging with TRC105(Fab)-conjugated, dual-labeled mesoporous silica nanoparticles. *Mol Pharm*. 2014;11(11):4007–4014.

48. Sun B, Ranganathan B, Feng SS. Multifunctional poly(D,L-lactide-co-glycolide)/montmorillonite (PLGA/MMT) nanoparticles decorated by Trastuzumab for targeted chemotherapy of breast cancer. *Biomaterials*. 2008;29(4):475–486.

49. Milgroom A, Intrator M, Madhavan K, et al. Mesoporous silica nanoparticles as a breast-cancer targeting ultrasound contrast agent. *Colloids Surf B Biointerfaces*. 2014;116:652–657.